Search for $B^0 \to K^{*0}\tau^+\tau^-$ Decays at the Belle II Experiment

I. Adachi, K. Adamczyk, L. Aggarwal, H. Ahmed, H. Aihara, N. Akopov, M. Alhakami, A. Aloisio, N. Althubiti, M. Angelsmark, N. Anh Ky, D. M. Asner, H. Atmacan, V. Aushev, M. Aversano, R. Ayad, V. Babu, H. Bae, N. K. Baghel, S. Bahinipati, P. Bambade, Sw. Banerjee, S. Bansal, M. Barrett, M. Bartl, J. Baudot, A. Baur, A. Beaubien, F. Becherer, J. Becker, J. V. Bennett, F. U. Bernlochner, V. Bertacchi, M. Bertemes, E. Bertholet, M. Bessner, S. Bettarini, V. Bhardwaj, B. Bhuyan, F. Bianchi, T. Bilka, D. Biswas, A. Bobrov, D. Bodrov, A. Bolz, A. Bondar, A. Boschetti, A. Bozek, M. Bračko, P. Branchini, N. Brenny, R. A. Briere, T. E. Browder, A. Budano, S. Bussino, Q. Campagna, M. Campajola, L. Cao, G. Casarosa, C. Cecchi, J. Cerasoli, M.-C. Chang, P. Chang, R. Cheaib, P. Cheema, B. G. Cheon, K. Chilikin, J. Chin, K. Chirapatpimol, H.-E. Cho, K. Cho, S.-J. Cho, S.-K. Choi, S. Choudhury, J. Cochran, I. Consigny, L. Corona, J. X. Cui, E. De La Cruz-Burelo, S. A. De La Motte, G. de Marino, G. De Nardo, G. De Pietro, R. de Sangro, M. Destefanis, S. Dey, R. Dhamija, A. Di Canto, F. Di Capua, J. Dingfelder, Z. Doležal, I. Domínguez Jiménez, T. V. Dong, M. Dorigo, D. Dossett, S. Dubey, K. Dugic, G. Dujany, P. Ecker, D. Epifanov, J. Eppelt, P. Feichtinger, T. Ferber, T. Fillinger, C. Finck, G. Finocchiaro, A. Fodor, F. Forti, B. G. Fulsom, A. Gabrielli, E. Ganiev, M. Garcia-Hernandez, R. Garg, G. Gaudino, V. Gaur, V. Gautam, A. Gaz, A. Gellrich, G. Ghevondyan, D. Ghosh, H. Ghumaryan, G. Giakoustidis, R. Giordano, A. Giri, P. Gironella Gironell, A. Glazov, B. Gobbo, R. Godang, O. Gogota, P. Goldenzweig, W. Gradl, S. Granderath, E. Graziani, D. Greenwald, Z. Gruberová, Y. Guan, K. Gudkova, I. Haide, Y. Han, T. Hara, C. Harris, K. Hayasaka, H. Hayashii, S. Hazra, C. Hearty, M. T. Hedges, A. Heidelbach, I. Heredia de la Cruz, M. Hernández Villanueva, T. Higuchi, M. Hoek, M. Hohmann, R. Hoppe, P. Horak, C.-L. Hsu, T. Humair, T. Iijima, K. Inami, G. Inguglia, N. Ipsita, A. Ishikawa, R. Itoh, M. Iwasaki, P. Jackson, D. Jacobi, W. W. Jacobs, D. E. Jaffe, E.-J. Jang, Q. P. Ji, S. Jia, Y. Jin, A. Johnson, K. K. Joo, H. Junkerkalefeld, D. Kalita, A. B. Kaliyar, J. Kandra, K. H. Kang, S. Kang, G. Karyan, T. Kawasaki, F. Keil, C. Ketter, C. Kiesling, C.-H. Kim, D. Y. Kim, J.-Y. Kim, K.-H. Kim, Y.-K. Kim, H. Kindo, K. Kinoshita, P. Kodyš, T. Koga, S. Kohani, K. Kojima, A. Korobov, S. Korpar, E. Kovalenko, R. Kowalewski, P. Križan, P. Krokovny, T. Kuhr, Y. Kulii, D. Kumar, J. Kumar, R. Kumar, K. Kumara, T. Kunigo, A. Kuzmin, Y.-J. Kwon, S. Lacaprara, Y.-T. Lai, K. Lalwani, T. Lam, J. S. Lange, T. S. Lau, M. Laurenza, R. Leboucher, F. R. Le Diberder, M. J. Lee, C. Lemettais, P. Leo, P. M. Lewis, C. Li, L. K. Li, Q. M. Li, W. Z. Li, Y. Li, Y. B. Li, Y. P. Liao, J. Libby, J. Lin, S. Lin, M. H. Liu, Q. Y. Liu, Y. Liu, Z. Q. Liu, D. Liventsev, S. Longo, T. Lueck, C. Lyu, Y. Ma, C. Madaan, M. Maggiora, S. P. Maharana, R. Maiti, G. Mancinelli, R. Manfredi, E. Manoni, M. Mantovano, D. Marcantonio, S. Marcello, C. Marinas, C. Martellini, A. Martens, A. Martini, T. Martinov, L. Massaccesi, M. Masuda, K. Matsuoka, D. Matvienko, S. K. Maurya, M. Maushart, J. A. McKenna, R. Mehta, F. Meier, D. Meleshko, M. Merola, C. Miller, M. Mirra, S. Mitra, K. Miyabayashi, H. Miyake, R. Mizuk, G. B. Mohanty, S. Mondal, S. Moneta, H.-G. Moser, I. Nakamura, K. R. Nakamura, M. Nakao, H. Nakazawa, Y. Nakazawa, M. Naruki, Z. Natkaniec, A. Natochii, M. Nayak, G. Nazaryan, M. Neu, S. Nishida, S. Ogawa, R. Okubo, H. Ono, Y. Onuki, F. Otani, P. Pakhlov, G. Pakhlova, E. Paoloni, S. Pardi, K. Parham, H. Park, J. Park, K. Park, S.-H. Park, B. Paschen, A. Passeri, S. Patra, T. K. Pedlar, I. Peruzzi, R. Peschke, R. Pestotnik, M. Piccolo, L. E. Piilonen, P. L. M. Podesta-Lerma, T. Podobnik, S. Pokharel, A. Prakash, C. Praz, S. Prell, E. Prencipe, M. T. Prim, S. Privalov, I. Prudiiev, H. Purwar, P. Rados, G. Raeuber, S. Raiz, N. Rauls, K. Ravindran, J. U. Rehman, M. Reif, S. Reiter, M. Remnev, L. Reuter, D. Ricalde Herrmann, I. Ripp-Baudot, G. Rizzo, S. H. Robertson, M. Roehrken, J. M. Roney, A. Rostomyan, N. Rout, D. A. Sanders, S. Sandilya, L. Santelj, V. Savinov, B. Scavino, J. Schmitz, S. Schneider, M. Schnepf, C. Schwanda, Y. Seino, A. Selce, K. Senyo, J. Serrano, M. E. Sevior, C. Sfienti, W. Shan, C. Sharma, G. Sharma, X. D. Shi, T. Shillington, T. Shimasaki, J.-G. Shiu, D. Shtol, B. Shwartz, A. Sibidanov, F. Simon, J. B. Singh, J. Skorupa, R. J. Sobie, M. Sobotzik, A. Soffer, A. Sokolov, E. Solovieva, W. Song, S. Spataro, B. Spruck, M. Starič, P. Stavroulakis, S. Stefkova, R. Stroili, J. Strube, Y. Sue, M. Sumihama, K. Sumisawa, W. Sutcliffe, N. Suwonjandee, H. Svidras, M. Takahashi, M. Takizawa, U. Tamponi, K. Tanida, F. Tenchini, A. Thaller, O. Tittel, R. Tiwary, E. Torassa, K. Trabelsi, I. Tsaklidis, I. Ueda,

T. Uglov, K. Unger, Y. Unno, K. Uno, S. Uno, P. Urquijo, Y. Ushiroda, S. E. Vahsen, R. van Tonder, K. E. Varvell, M. Veronesi, A. Vinokurova, V. S. Vismaya, L. Vitale, V. Vobbilisetti, R. Volpe, A. Vossen, M. Wakai, S. Wallner, M.-Z. Wang, X. L. Wang, Z. Wang, A. Warburton, M. Watanabe, S. Watanuki, C. Wessel, E. Won, X. P. Xu, B. D. Yabsley, S. Yamada, W. Yan, W. C. Yan, J. Yelton, J. H. Yin, K. Yoshihara, C. Z. Yuan, J. Yuan, Y. Yusa, L. Zani, F. Zeng, M. Zeyrek, B. Zhang, J. S. Zhou, Q. D. Zhou, L. Zhu, V. I. Zhukova, and R. Žlebčík

(Belle II Collaboration)

(Received 16 April 2025; accepted 25 August 2025; published 6 October 2025)

We present a search for the rare flavor-changing neutral-current decay $B^0 \to K^{*0}\tau^+\tau^-$ with data collected by the Belle II experiment at the SuperKEKB electron-positron collider. The analysis uses a 365 fb^{-1} data sample recorded at the center-of-mass energy of the $\Upsilon(4S)$ resonance. One of the B mesons produced in the $\Upsilon(4S) \to B^0\bar{B}^0$ process is fully reconstructed in a hadronic decay mode, while its companion B meson is required to decay into a K^{*0} and two τ leptons of opposite charge. The τ leptons are reconstructed in final states with a single electron, muon, charged pion or charged ρ meson, and additional neutrinos. We set an upper limit on the branching fraction of $\mathcal{B}(B^0 \to K^{*0}\tau^+\tau^-) < 1.8 \times 10^{-3}$ at the 90% confidence level, which is the most stringent constraint reported to date.

DOI: 10.1103/v1q3-9dy8

In the standard model (SM) $b \to s\tau\tau$ transitions occur only at the loop level via penguin or box diagrams, and are therefore suppressed. Combining the charged and neutral $B \to K^*\tau^+\tau^-$ modes [1], the predicted SM branching fraction in the $(15, 19)$ GeV$/c^2$ dilepton invariant mass-squared range is $(0.98 \pm 0.10) \times 10^{-7}$ [2,3]. New physics models can enhance $b \to s\tau\tau$ rates by up to 3 orders of magnitude [3]. In some scenarios, the leading new physics couplings are those involving the third-fermion generation, making $b \to s\tau\tau$ transitions a better probe than $b \to see$ and $b \to s\mu\mu$ [4]. Enhancements to $b \to s\tau\tau$ are also foreseen in models that explain the recently observed 2.7σ departure from the SM expectation in the $B^+ \to K^+\nu\bar{\nu}$ decay rate [5,6], together with the $b \to c\tau\nu$ anomalies [3,7].

The Belle experiment has reported an upper limit at the 90% confidence level on the $B^0 \to K^{*0}\tau^+\tau^-$ branching fraction of 3.1×10^{-3}, using a 711 fb^{-1} data sample recorded at the $\Upsilon(4S)$ resonance and reconstructing the accompanying B meson in fully hadronic decay modes [8]. Other $b \to s\tau\tau$ searches have been conducted by *BABAR* [9] and LHCb [10]. None of these searches led to evidence for a signal, and all the upper limits are above the SM predictions.

We report a search for $B^0 \to K^{*0}\tau^+\tau^-$ [11] decay at Belle II. The main challenge is the presence of up to four final-state neutrinos. Reconstructing one B meson ($B_{\rm tag}$) in $e^+e^- \to \Upsilon(4S) \to B\bar{B}$ isolates the accompanying B meson ($B_{\rm sig}$) and constrains the kinematics of the missing neutrinos. We reconstruct the $B_{\rm tag}$ in hadronic decay modes and search for a $B^0 \to K^{*0}\tau^+\tau^-$ decay of the partner $B_{\rm sig}$, where the $K^{*0} \to K^+\pi^-$ mode is used. All the combinations of the decay modes $\tau^- \to e^-\bar{\nu}_e\nu_\tau$, $\tau^- \to \mu^-\bar{\nu}_\mu\nu_\tau$, $\tau^- \to \pi^-\nu_\tau$, and $\tau^- \to \rho^-\nu_\tau$ are utilized for the two τ's. A multivariate approach with a binary classifier is adopted to separate signal from background events. The classifier output is used in a binned profile-likelihood fit to extract the signal branching fraction. To minimize experimental bias, we finalized the full analysis procedure before examining the data in the signal region. The main new features compared to the previous $B^0 \to K^{*0}\tau^+\tau^-$ search [8] are the use of an improved tagging method [12], the adoption of a multivariate approach instead of a cut-based one, and the inclusion of $\tau^- \to \rho^-\nu_\tau$ decay modes. The Belle II analysis described here improves the expected sensitivity by a factor of 2.6, despite using a smaller dataset.

We use a 365 fb^{-1} data sample recorded by the Belle II detector, located at the SuperKEKB asymmetric electron-positron collider [13], between 2019 and 2022. The data are collected at a center-of-mass (c.m.) energy $\sqrt{s} = 10.58$ GeV, corresponding to the peak of the $\Upsilon(4S)$ resonance. An additional 43 fb^{-1} data sample, collected at a c.m. energy 60 MeV below the mass of the $\Upsilon(4S)$ resonance (off-resonance), is used to study backgrounds from $e^+e^- \to q\bar{q}$ events, where q indicates a u, d, s, or c quark. The Belle II detector [14] consists of a nearly hermetic magnetic spectrometer, composed of silicon detectors and a central drift chamber (CDC),

surrounded by particle identification (PID), electromagnetic calorimetry (ECL), and muon and K_L^0 subdetectors. Simulated samples are used to suppress backgrounds, estimate the signal efficiency, and define fit templates for the branching fraction extraction. Various Monte Carlo (MC) event generators are utilized. The EvtGen [15], Pythia8 [16], KKMC [17], and TAUOLA [18] software packages are used to model particle production and decay, PHOTOS [19] is used for photon radiation from final-state charged particles, and Geant4 [20] simulates material interaction and detector response. We simulate $B^0 \to K^{*0}\tau^+\tau^-$ signal decays using SM form factor calculations from Ref. [21]; we generate only the final state with $K^{*0} \to K^+\pi^-$, and we take this into account in the signal efficiency calculation. Simulated beam-induced backgrounds are overlaid onto the events [22]. The Belle II analysis software framework [23,24] is used for event reconstruction.

The analysis starts by reconstructing a $B_{\rm tag}$ into one of 32 hadronic B^0 decay modes using the full event interpretation algorithm (FEI) [12], in which final-state particles, reconstructed from tracks and energy deposits in the ECL (clusters), are combined into intermediate particles until the final $B_{\rm tag}$ candidates are formed. For each decay chain, the algorithm calculates the probability ($P_{\rm FEI}$) that the reconstructed decay mode is correct, using gradient-boosted decision trees [25]. Known $B_{\rm tag}$ kinematic properties can be exploited using the beam-energy-constrained mass $M_{\rm bc} = \sqrt{s/(2c^2)^2 - |\vec{p}^{\,*}_{B_{\rm tag}}/c|^2}$ and the energy difference $\Delta E = E^*_{B_{\rm tag}} - \sqrt{s}/2$, where $\vec{p}^{\,*}_{B_{\rm tag}}$ and $E^*_{B_{\rm tag}}$ represent the momentum and energy of the $B_{\rm tag}$ in the c.m. frame, respectively. Correctly reconstructed B mesons peak in the $M_{\rm bc}$ distribution at the known B^0 mass and have values close to zero for ΔE. We select $B_{\rm tag}$ candidates with $M_{\rm bc} > 5.27\,{\rm GeV}/c^2$, $|\Delta E| < 200$ MeV, and $P_{\rm FEI} > 0.01$. At this stage, for the simulated signal sample, 0.9% of events are retained, with an average multiplicity of 1.5 $B_{\rm tag}$ candidates. To minimize possible mismodeling in the $B_{\rm tag} - B_{\rm sig}$ combination step, for each event only the $B_{\rm tag}$ candidate with the highest value of $P_{\rm FEI}$ is retained. In the signal MC sample, this selection picks the correctly reconstructed $B_{\rm tag}$ candidate about 87% of the time.

Tracks and clusters not associated to the selected $B_{\rm tag}$ are used to reconstruct $B_{\rm sig}$ candidates. Spurious tracks from beam-induced background are rejected by selecting only the tracks that originate close to the interaction point by requiring small transverse and longitudinal impact parameters, $dr < 2\,{\rm cm}$ and $|dz| < 4\,{\rm cm}$, respectively. Furthermore, tracks should have polar angles in the CDC acceptance ($17° < \theta < 150°$) and transverse momenta $p_T > 100\,{\rm MeV}/c$. In order to have a reliable ${\rm d}E/{\rm d}x$ measurement for PID, only tracks having at least 20 CDC hits are retained. For each track, a charged particle hypothesis is assigned using PID selectors, which combine information from the different subdetectors. A likelihood-based binary classifier separates charged pions from kaons. For muon identification, a likelihood-based selector is used as well, while for electrons a selector based on a boosted decision tree (BDT) [26] is applied. We choose selection thresholds resulting in efficiencies of 95% for hadrons, 82% for electrons, and 77% for muons; in the selected sample, 6%, 3%, and 30% of the respective candidates are misidentified, according to the $B^0 \to K^{*0}\tau^+\tau^-$ simulation. PID selection efficiencies and misidentification probabilities are evaluated via data control channels in bins of momentum and polar angle of the reconstructed particles [5,27]. Simulated events are weighted to correct for the differences compared to the data. Clusters that are not matched to any extrapolated track, and have polar angles in the CDC acceptance, are used to identify photon candidates. We reconstruct π^0 candidates using photons with energy thresholds of 80, 30, and 60 MeV in the forward, barrel, and backward region of the ECL, respectively. These thresholds are optimized to suppress background from high multiplicity B decays. Photon pairs are then combined if their invariant mass is in the range $(120, 145)\ {\rm MeV}/c^2$, corresponding to approximately 2 times the experimental resolution around the known π^0 mass [28], and their maximum angular separation is 1.5 rad in the transverse plane and 1.4 rad in the 3D space. The selection criteria result in a π^0 reconstruction efficiency of about 30%. The π^0 reconstruction efficiency is computed in bins of π^0 momentum using data control samples from D and τ decays. The observed differences between data and simulation are used to correct the simulated distributions. The π^0 candidates are then used to construct $\rho^- \to \pi^-\pi^0$ candidates. We require an invariant mass in the range $(0.65, 0.9)\ {\rm GeV}/c^2$, which is chosen to reduce the contamination from combinatorial background. Pairs of charged kaons and pions having opposite charges are combined to form $K^{*0} \to K^+\pi^-$ candidates if their invariant mass is in the range $(0.80, 0.99)\ {\rm GeV}/c^2$, corresponding to 4 times the K^{*0} decay width. A vertex fit [29] constrains the two tracks to originate from a common vertex, which is identified as the K^{*0} candidate decay point. Candidate K^{*0} mesons that have a p value for the vertex fit smaller than 10^{-3} are rejected.

Each $B_{\rm sig}$ candidate is formed by combining a reconstructed K^{*0} with the daughters of two oppositely charged τ leptons, in combinations of e^-, μ^-, π^-, and ρ^-. The daughters of the two τ leptons are henceforth denoted as t_1 and t_2, where t_1 has the same charge sign as the charged kaon from the K^{*0}. A total of 16 possible combinations of $t_1 t_2$ final states are examined. The invariant mass of the K^{*0}, t_1, and t_2 system should be less than 6.0 ${\rm GeV}/c^2$, to reject badly misreconstructed combinations.

Multiple $B_{\rm sig}$ candidates can be reconstructed for a single event. At this stage, all the $B_{\rm sig}$ candidates are retained and combined with the unique $B_{\rm tag}$, to form $\Upsilon(4S)$ candidates.

For each $\Upsilon(4S)$ candidate, the rest of the event (ROE) contains all the remaining tracks and clusters not used either for B_{tag} or for B_{sig} reconstruction. We require zero charged tracks in the ROE. The track selection in the ROE is the same as for the signal candidate except that the requirement on the number of CDC hits is removed. The selection of clusters in the ROE also follows the procedure adopted for B_{sig} photons, with energy thresholds of 100, 60, and 150 MeV in the forward, barrel, and backward regions of the ECL, respectively, optimized to reject clusters from beam background. We also require no track trajectory extrapolating to the ECL in a 20 cm radius around the cluster center. The latter requirement suppresses background clusters due to secondary particles generated in nuclear interactions of hadrons with the ECL material. We define the extra energy (E_{extra}) as the sum of the energies of all the clusters assigned to the ROE.

To reduce the contamination from events with particles outside of the acceptance of the tracking detectors, the polar angle of the missing momentum should be inside the CDC angular acceptance. The missing four-momentum of the event is defined as $p_{\text{miss}} = p_{\text{init}} - \sum_i p_i$, where p_{init} is the initial total four-momentum of the colliding beams, and the sum runs over the four-momenta of all the tracks and all the clusters in the ECL without an associated track. The flavor of the reconstructed B_{sig}, determined by the charge of the kaon from the K^{*0} decay, is required to be opposite to the flavor of the partner B_{tag} candidate. The opposite correlation is also used to define the "same-flavor" control sample, with reconstructed B^0B^0 and $\bar{B}^0\bar{B}^0$ pairs. This sample also includes signal events in which one of the two B^0 mesons has undergone flavor mixing before decaying, with a mixing probability $\chi_d = 18.6\%$ [28], resulting in a signal contamination below the expected sensitivity of the analysis. The $B^0 \to K^{*0}\tau^+\tau^-$ signal efficiency at this stage is 4.9×10^{-4} with an expected background yield of 98.4×10^3 events, about 35% of which are $e^+e^- \to \Upsilon(4S) \to B^0\bar{B}^0$ events. The next largest source of background, about 30% of the total, is from $e^+e^- \to c\bar{c}$ continuum processes.

The kinematic features of the signal side depend on the decay modes of the two τ leptons. Therefore, we separate the reconstructed events into four signal categories: three t_1t_2 categories, namely $\ell\ell$, $\pi\ell$, and $\pi\pi$, where $t_1, t_2 = \ell, \pi$ indicates the τ daughter, and the ρ category, in which one τ decays as $\tau^- \to \rho^-\nu_\tau$, while the other τ decays to any of the four reconstructed modes. The first three categories differ in the number of neutrinos in the final state. The ρ category can have one or two reconstructed π^0's from B_{sig}, while the number of neutrinos is not fixed. In the simulated signal sample, the average $\Upsilon(4S)$ candidate multiplicity per event is 4.4, and the fraction of events with one correctly reconstructed B_{sig} candidate is 77%. To avoid double counting due to cross-feed among signal categories, we select a single $\Upsilon(4S)$ candidate in each event, as follows.

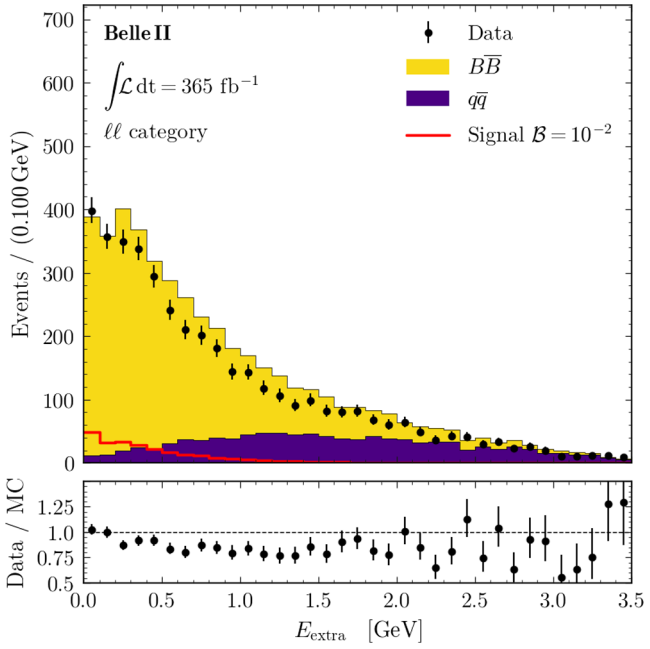

FIG. 1. Distribution of E_{extra} for events passing the nominal selection, with all the corrections applied, for the $\ell\ell$ signal category. The signal $B^0 \to K^{*0}\tau^+\tau^-$ histogram is shown scaled assuming a branching fraction of 10^{-2}.

First, we select the $\Upsilon(4S)$ candidate(s) having the closest K^{*0} mass to the measured value [28]. If a reconstructed $\rho^- \to \pi^-\pi^0$ is present in the event, we retain only the candidates assigned to the ρ category to prevent the π^0 from contributing to the ROE. Candidates with more identified electrons or muons are then selected to maintain a high signal efficiency for the purest categories. At this stage, the average $\Upsilon(4S)$ candidate multiplicity in each event is 1.3, and for the events that have multiple candidates, the final choice is performed randomly. A comparison using a fully random selection of the $\Upsilon(4S)$ candidate shows that the procedure outlined above results in a 15% higher fraction of correctly reconstructed signal events, with no bias introduced in the observables used for the signal extraction.

A control sample with a clean $B^0 \to K^{*0}J/\psi(\to\mu^+\mu^-)$ decay is used to validate the simulated $B^0 \to K^{*0}\tau^+\tau^-$ signal, using the same strategy described in [5]. The tracks and clusters associated with the $J/\psi K^{*0}$ candidate are replaced with those originating from a $K^{*0}\tau^+\tau^-$ decay, extracted from simulated $B^0 \to K^{*0}\tau^+\tau^-$ events, so that only the B_{tag} and the ROE's are taken from the control sample. The ratio of data to simulation efficiencies is found to be 0.81 ± 0.09 and the central value is used as a correction for the $B^0 \to K^{*0}\tau^+\tau^-$ signal efficiency. The same factor is also used to scale the $B^0\bar{B}^0$ background events having a correctly reconstructed B_{tag} (peaking $B^0\bar{B}^0$). The remaining portion of the $B\bar{B}$ events (combinatorial $B\bar{B}$) is normalized with the same-flavor control sample. The same-flavor sample is also used to correct the

TABLE I. Signal efficiencies (ε) and expected background yields for $\eta(\mathrm{BDT}) > 0.4$. The uncertainty on ε is dominated by the signal normalization systematic. The signal categories are ordered according to the expected sensitivity.

Signal category	$\varepsilon \times 10^5$	$B\bar{B}$	$q\bar{q}$
$\ell\ell$	4.0 ± 0.6	275	39
$\pi\ell$	7.6 ± 1.1	1058	230
ρ	15.5 ± 2.2	3279	845
$\pi\pi$	4.0 ± 0.6	1077	424

ROE cluster multiplicity, separately for each signal category, since MC simulation mismodeling affects the E_{extra} distribution. Figure 1 shows the E_{extra} distribution for the $\ell\ell$ category with the ROE cluster multiplicity correction applied. The residual data-MC discrepancies for $E_{\mathrm{extra}} > 200$ MeV are covered by the systematic uncertainties, described below. The normalization of $e^+e^- \to q\bar{q}$ backgrounds events is adjusted for each signal category using the off-resonance data sample.

We separate signal from background through BDT binary classifiers [30], trained on simulated samples, separately for each signal category. Each BDT uses the same set of 14 variables, selected based on their discriminating power and on the level of data-simulation agreement observed in the same-flavor control sample. These variables combine information about the event shape, the kinematics of K^{*0} and τ candidates, the missing four-momentum, and E_{extra}. In addition, the invariant masses $M(K^{*0}; t_i)$, $i = 1, 2$ are used as inputs to target $B \to D^{(*)}\ell\nu$ backgrounds. The most discriminating input variables are the missing energy, E_{extra}, $M(K^{*0}; t_i)$, and $q^2 = (p_{\tau^+} + p_{\tau^-})^2$ [31]. To use the entire simulated sample, we perform a twofold training: the samples are randomly split into two halves, and the classifier is trained separately on each half. The set of model weights obtained from each training are then applied to the complementary half sample. Good agreement between the outputs of the two trainings is observed.

The range [0.4, 1] of the BDT output [$\eta(\mathrm{BDT})$], defined as signal region (SR), is used in the fit for the branching fraction. The SR is common to all signal categories and is determined by the need to maintain high signal efficiency while limiting the impact of background-related systematic uncertainties on the expected branching fraction. Table I gives the signal efficiencies (ε) and the expected background composition in the SR. The $\ell\ell$ category is the most sensitive. In this category, the largest background contamination comes from $B\bar{B}$, 60% of which are peaking $B^0\bar{B}^0$ pairs. In about 45% of the $B\bar{B}$ events, a neutral B_{tag} is correctly reconstructed while the other B^0 decays to a semileptonic or semitauonic final state. This fraction is lower for the other signal categories and is 20% for the $\pi\pi$ one.

The signal branching fraction is extracted from an binned maximum likelihood fit to the $\eta(\mathrm{BDT})$ distribution in the SR, simultaneously for all four signal categories, using the PYHF [32,33] and the Cabinetry libraries [34]. The parameter of interest is $\mathcal{B}(B^0 \to K^{*0}\tau^+\tau^-) = N_{\mathrm{sig}}/(2\varepsilon N_{\Upsilon(4S)} f_{00})$, where $N_{\Upsilon(4S)} = (387 \pm 6) \times 10^6$ is the number of produced $\Upsilon(4S)$, estimated from a data-driven approach in which non-$\Upsilon(4S)$ events are subtracted from on-resonance data, and $f_{00} = 0.4861^{+0.0074}_{-0.0080}$ [7] is the $\Upsilon(4S) \to B^0\bar{B}^0$ decay rate. A uniform bin width is chosen for each signal category, such that each bin contains more than 10 expected background events. The templates for the fit components (signal, $B\bar{B}$, and $q\bar{q}$ backgrounds) are obtained from simulated samples.

The parameter of interest is unconstrained in the fit, while systematic uncertainties are incorporated into the likelihood as nuisance parameters with Gaussian constraints. The uncertainties on the correction factors for the pion, kaon, and lepton identification efficiencies and misidentification probabilities, as well as for the π^0

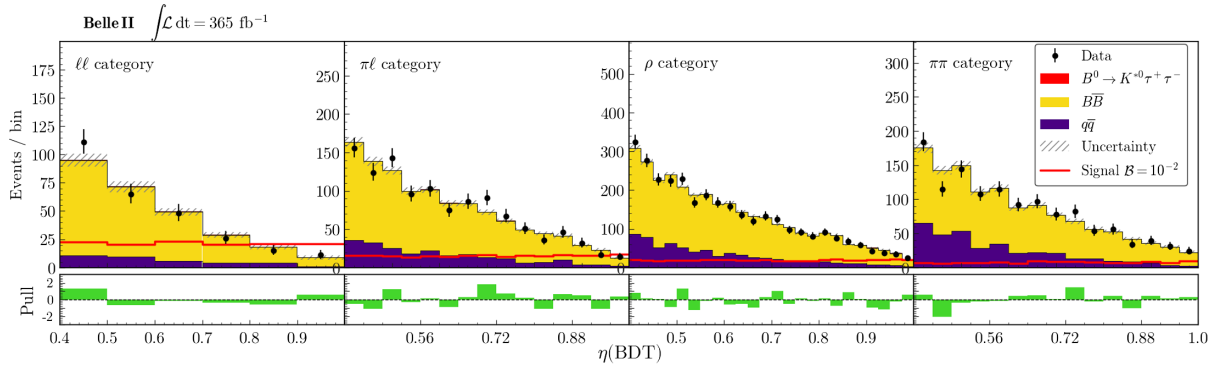

FIG. 2. Distributions of $\eta(\mathrm{BDT})$ in the SR for the four signal categories. The fit results are shown for the two background components ($B\bar{B}$ and $q\bar{q}$) and the $B^0 \to K^{*0}\tau^+\tau^-$ signal, with a fitted branching fraction of $[-0.15 \pm 1.01] \times 10^{-3}$. A $B^0 \to K^{*0}\tau^+\tau^-$ signal distribution, scaled assuming a branching fraction of 10^{-2}, is shown as reference. The bottom panel shows the pull distributions. The histograms for the four categories are available on HEPData [37].

efficiency, are determined from the auxiliary measurements, as described above. We assign a systematic uncertainty to the correction of the ROE cluster multiplicity. The uncertainty is taken to be 100% of the residual difference in the data-to-simulation ratio observed in the $\eta(\mathrm{BDT}) < 0.4$ control region, after applying the correction derived from the same-flavor sample. The branching fractions of decay modes contributing to about 70% of B^0 decays and 50% of B^+ decays in the SR are allowed to vary according to their known uncertainties [28]. We assign a 50% uncertainty on the branching fractions of $B \to D^{**}\ell/\tau\nu$ decays, which are poorly known and constitute about 5% (9%) of the residual $B^0\bar{B}^0$ (B^+B^-) background. The $B\bar{B}$ events in which a D meson decays to a final state with a K_L^0 are scaled by 1.30, and a 10% systematic uncertainty is assigned to them [5]. The normalization factors for $q\bar{q}$, combinatorial $B\bar{B}$, peaking $B^0\bar{B}^0$ backgrounds, and signal efficiency are evaluated in the SR using the same control samples previously described, and they are found to be consistent with the values determined in the full $\eta(\mathrm{BDT})$ region. Thus no further correction is applied. The relative statistical uncertainty on the correction, as derived from the control samples, is assigned as a systematic uncertainty, as described below. An uncertainty on the normalization factor for the $q\bar{q}$ background, due to the statistical uncertainty of the off-resonance sample and ranging from 70% for the $\ell\ell$ mode to 15% for the ρ and $\pi\pi$ signal categories, is assigned. The combinatorial $B\bar{B}$ yield is allowed to vary by 15%, while the peaking $B^0\bar{B}^0$ and signal normalizations are assumed to be known at the 14% level. We use a dedicated $B^0 \to K^{*0}\tau^+\tau^-$ MC sample, generated with a modified parametrization of the form factors [21], to evaluate the systematic uncertainty due to the knowledge of signal form factors. Global normalization uncertainties on the luminosity measurement (0.5%), the number of $\Upsilon(4S)$ (1.5%), and the f_{00} parameter $(^{+1.5\%}_{-1.6\%})$ are treated with one nuisance parameter each. Finally, the systematic uncertainty due to the limited size of simulated samples is also taken into account.

Before examining the SR, we validate the fit procedure with MC pseudoexperiments, in which both statistical and systematic uncertainties are taken into account. No bias in the branching fraction and its uncertainty is observed, with an injected signal branching fraction ranging from zero to the current upper limit value [8]. As an additional check, a set of pseudoexperiments is constructed by varying the number of expected events in each bin of the fit variable. The variations are derived from the data-simulation discrepancies observed in those bins for the same-flavor control sample. Again in this case, no bias is observed when performing a fit. Assuming the background-only hypothesis, the expected branching fraction uncertainty on simulated events is computed to be 0.98×10^{-3}. This corresponds to an expected 90% confidence level (C.L.) upper limit of 1.7×10^{-3}, which was determined using the CLs method [35], a modified frequentist approach that is based on a profile-likelihood ratio [36].

TABLE II. The systematic uncertainties for the branching fraction of $B^0 \to K^{*0}\tau^+\tau^-$, which were computed following the procedure in Ref. [38].

Source	Impact on $\mathcal{B} \times 10^{-3}$
$B \to D^{**}\ell/\tau\nu$ branching fractions	0.29
Simulated sample size	0.27
$q\bar{q}$ normalization	0.18
ROE cluster multiplicity	0.17
π and K ID	0.14
B decay branching fraction	0.11
Combinatorial $B\bar{B}$ normalization	0.09
Signal and peaking $B^0\bar{B}^0$ normalization	0.07
Lepton ID	0.04
π^0 efficiency	0.03
f_{00}	0.01
$N_{\Upsilon(4S)}$	0.01
$D \to K_L^0$ decays	0.01
Signal form factors	0.01
Luminosity	<0.01
Total systematics	0.52
Statistics	0.86

The result of the fit to data is shown in Fig. 2, corresponding to a measured branching fraction of $\mathcal{B}(B^0 \to K^{*0}\tau^+\tau^-) = [-0.15 \pm 0.86(\mathrm{stat}) \pm 0.52(\mathrm{syst})] \times 10^{-3}$. The distributions of $\eta(\mathrm{BDT})$ in the SR for the four signal categories are available on HEPData [37]. Compatibility between the data and fit result is assessed using simplified MC pseudoexperiments, and a p value of 48.3% is obtained. The measurement is statistically limited. The impact of the various systematic uncertainties on the branching fraction is given in Table II; the knowledge of the $B \to D^{**}\ell/\tau\nu$ decays' branching fractions and the simulated sample size are the largest contributions. As no significant signal is observed, we obtain a 90% C.L. upper limit of 1.8×10^{-3}.

In summary, we present the first search for the $B^0 \to K^{*0}\tau^+\tau^-$ decays at Belle II, utilizing the hadronic tagging technique. We analyze a 365 fb^{-1} dataset collected by the Belle II experiment at the SuperKEKB e^+e^- collider. No evidence for a signal is observed, and an upper limit on the branching fraction of 1.8×10^{-3} at the 90% confidence level is set, assuming a signal with SM-like properties. This is the most stringent limit on the $B^0 \to K^{*0}\tau^+\tau^-$ decay to date.

Acknowledgments—This work, based on data collected using the Belle II detector, which was built and commissioned prior to March 2019, was supported by Higher Education and Science Committee of the Republic of Armenia Grant No. 23LCG-1C011; Australian Research

Council and Research Grants No. DP200101792, No. DP210101900, No. DP210102831, No. DE220100462, No. LE210100098, and No. LE230100085; Austrian Federal Ministry of Education, Science and Research, Austrian Science Fund (FWF) Grants DOI: 10.55776/P34529, DOI: 10.55776/J4731, DOI: 10.55776/J4625, DOI: 10.55776/M3153, and DOI: 10.55776/PAT1836324, and Horizon 2020 ERC Starting Grant No. 947006 "InterLeptons"; Natural Sciences and Engineering Research Council of Canada, Compute Canada and CANARIE; National Key R&D Program of China under Contract No. 2022YFA1601903, National Natural Science Foundation of China and Research Grants No. 11575017, No. 11761141009, No. 11705209, No. 11975076, No. 12135005, No. 12150004, No. 12161141008, No. 12475093, and No. 12175041, and Shandong Provincial Natural Science Foundation Project ZR2022JQ02; the Czech Science Foundation Grant No. 22-18469S and Charles University Grant Agency Project No. 246122; European Research Council, Seventh Framework PIEF-GA-2013-622527, Horizon 2020 ERC-Advanced Grants No. 267104 and No. 884719, Horizon 2020 ERC-Consolidator Grant No. 819127, Horizon 2020 Marie Sklodowska-Curie Grant Agreements No. 700525 "NIOBE" and No. 101026516, and Horizon 2020 Marie Sklodowska-Curie RISE project JENNIFER2 Grant Agreement No. 822070 (European grants); L'Institut National de Physique Nucléaire et de Physique des Particules (IN2P3) du CNRS and L'Agence Nationale de la Recherche (ANR) under Grant No. ANR-21-CE31-0009 (France); BMBF, DFG, HGF, MPG, and AvH Foundation (Germany); Department of Atomic Energy under Project Identification No. RTI 4002, Department of Science and Technology, and UPES SEED funding programs No. UPES/R&D-SEED-INFRA/17052023/01 and No. UPES/R&D-SOE/20062022/06 (India); Israel Science Foundation Grant No. 2476/17, U.S.-Israel Binational Science Foundation Grant No. 2016113, and Israel Ministry of Science Grant No. 3-16543; Istituto Nazionale di Fisica Nucleare and the Research Grants BELLE2, and the ICSC—Centro Nazionale di Ricerca in High Performance Computing, Big Data and Quantum Computing, funded by European Union—NextGenerationEU; Japan Society for the Promotion of Science, Grant-in-Aid for Scientific Research Grants No. 16H03968, No. 16H03993, No. 16H06492, No. 16K05323, No. 17H01133, No. 17H05405, No. 18K03621, No. 18H03710, No. 18H05226, No. 19H00682, No. 20H05850, No. 20H05858, No. 22H00144, No. 22K14056, No. 22K21347, No. 23H05433, No. 26220706, and No. 26400255, and the Ministry of Education, Culture, Sports, Science, and Technology (MEXT) of Japan; National Research Foundation (NRF) of Korea Grants No. 2016R1-D1A1B-02012900, No. 2018R1-A6A1A-06024970, No. 2021R1-A6A1A-03043957, No. 2021R1-F1A-1060423, No. 2021R1-F1A-1064008, No. 2022R1-A2C-1003993, No. 2022R1-A2C-1092335, No. RS-2023-00208693, No. RS-2024-00354342, and No. RS-2022-00197659, Radiation Science Research Institute, Foreign Large-Size Research Facility Application Supporting project, the Global Science Experimental Data Hub Center, the Korea Institute of Science and Technology Information (K24L2M1C4) and KREONET/GLORIAD; Universiti Malaya RU grant, Akademi Sains Malaysia, and Ministry of Education Malaysia; Frontiers of Science Program Contracts No. FOINS-296, No. CB-221329, No. CB-236394, No. CB-254409, and No. CB-180023, and SEP-CINVESTAV Research Grant No. 237 (Mexico); the Polish Ministry of Science and Higher Education and the National Science Center; the Ministry of Science and Higher Education of the Russian Federation and the HSE University Basic Research Program, Moscow; University of Tabuk Research Grants No. S-0256-1438 and No. S-0280-1439 (Saudi Arabia), and Researchers Supporting Project (RSPD2025R873), King Saud University, Riyadh, Saudi Arabia; Slovenian Research Agency and Research Grants No. J1-9124 and No. P1-0135; Agencia Estatal de Investigacion, Spain Grant No. RYC2020-029875-I and Generalitat Valenciana, Spain Grant No. CIDEGENT/2018/020; The Knut and Alice Wallenberg Foundation (Sweden), Contracts No. 2021.0174 and No. 2021.0299; National Science and Technology Council, and Ministry of Education (Taiwan); Thailand Center of Excellence in Physics; TUBITAK ULAKBIM (Turkey); National Research Foundation of Ukraine, Project No. 2020.02/0257, and Ministry of Education and Science of Ukraine; the U.S. National Science Foundation and Research Grants No. PHY-1913789 and No. PHY-2111604, and the U.S. Department of Energy and Research Awards No. DE-AC06-76RLO1830, No. DE-SC0007983, No. DE-SC0009824, No. DE-SC0009973, No. DE-SC0010007, No. DE-SC0010073, No. DE-SC0010118, No. DE-SC0010504, No. DE-SC0011784, No. DE-SC0012704, No. DE-SC0019230, No. DE-SC0021274, No. DE-SC0021616, No. DE-SC0022350, No. DE-SC0023470; and the Vietnam Academy of Science and Technology (VAST) under Grants No. NVCC.05.12/22-23 and No. DL0000.02/24-25. We thank the SuperKEKB team for delivering high-luminosity collisions; the KEK cryogenics group for the efficient operation of the detector solenoid magnet and IBBelle on site; the KEK Computer Research Center for on-site computing support; the NII for SINET6 network support; and the raw-data centers hosted by BNL, DESY, GridKa, IN2P3, INFN, and the University of Victoria. These acknowledgements are not to be interpreted as an endorsement of any statement made by any of

our institutes, funding agencies, governments, or their representatives.

Data availability—Numerical data corresponding to the results presented are available as HEPData [37]. The full Belle II data are not publicly available. The collaboration will consider requests for access to the data that support this article.

[1] Henceforth, K^* indicates the $K^*(892)$ state.
[2] J. L. Hewett, Phys. Rev. D **53**, 4964 (1996).
[3] B. Capdevila, A. Crivellin, S. Descotes-Genon, L. Hofer, and J. Matias, Phys. Rev. Lett. **120**, 181802 (2018).
[4] C. Cornella, D. A. Faroughy, J. Fuentes-Martin, G. Isidori, and M. Neubert, J. High Energy Phys. 08 (2021) 050.
[5] I. Adachi *et al.* (Belle II Collaboration), Phys. Rev. D **109**, 112006 (2024).
[6] L. Allwicher, D. Becirevic, G. Piazza, S. Rosauro-Alcaraz, and O. Sumensari, Phys. Lett. B **848**, 138411 (2024).
[7] S. Banerjee *et al.* (HFLAV Collaboration), arXiv:2411.18639.
[8] T. V. Dong, T. Luo *et al.* (Belle Collaboration), Phys. Rev. D **108**, L011102 (2023).
[9] J. P. Lees, V. Poireau, V. Tisserand *et al.* (*BABAR* Collaboration), Phys. Rev. Lett. **118**, 031802 (2017).
[10] R. Aaij, B. Adeva, M. Adinolfi *et al.* (LHCb Collaboration), Phys. Rev. Lett. **118**, 251802 (2017).
[11] Charge conjugate modes are implied throughout the text.
[12] T. Keck *et al.*, Comput. Software Big Sci. **3**, 6 (2019).
[13] K. Akai, K. Furukawa, and H. Koiso, Nucl. Instrum. Methods Phys. Res., Sect. A **907**, 188 (2018).
[14] T. Abe (Belle II Collaboration), arXiv:1011.0352.
[15] D. J. Lange, Nucl. Instrum. Methods Phys. Res., Sect. A **462**, 152 (2001).
[16] T. Sjöstrand, S. Ask, J. R. Christiansen, R. Corke, N. Desai, P. Ilten, S. Mrenna, S. Prestel, C. O. Rasmussen, and P. Z. Skands, Comput. Phys. Commun. **191**, 159 (2015).
[17] S. Jadach, B. F. L. Ward, and Z. Wąs, Comput. Phys. Commun. **130**, 260 (2000).
[18] S. Jadach, J. H. Kuhn, and Z. Wąs, Comput. Phys. Commun. **64**, 275 (1990).
[19] E. Barberio and Z. Wąs, Comput. Phys. Commun. **79**, 291 (1994).
[20] S. Agostinelli *et al.* (GEANT4 Collaboration), Nucl. Instrum. Methods Phys. Res., Sect. A **506**, 250 (2003).
[21] A. Ali, P. Ball, L. T. Handoko, and G. Hiller, Phys. Rev. D **61**, 074024 (2000).
[22] A. Natochii *et al.*, arXiv:2203.05731.
[23] T. Kuhr, C. Pulvermacher, M. Ritter, T. Hauth, and N. Braun (Belle II Framework Software Group), Comput. Software Big Sci. **3**, 1 (2019).
[24] Belle II Collaboration, Belle II Analysis Software Framework (basf2), 10.5281/zenodo.5574115 (2025).
[25] T. Keck, Comput. Software Big Sci. **1**, 2 (2017).
[26] A. Hocker *et al.*, TMVA—Toolkit for multivariate data analysis with ROOT: Users guide. TMVA—Toolkit for multivariate data analysis, Technical Report No. CERN-OPEN-2007-007, CERN, Geneva, 2007.
[27] Belle II Collaboration, Report No. BELLE2-NOTE-PL-2020-027, 2020.
[28] S. Navas *et al.* (Particle Data Group), Phys. Rev. D **110**, 030001 (2024).
[29] J.-F. Krohn *et al.* (Belle II Analysis Software Group), Nucl. Instrum. Methods Phys. Res., Sect. A **976**, 164269 (2020).
[30] T. Chen and C. Guestrin, in *Proceedings of the 22nd ACM SIGKDD International Conference on Knowledge Discovery and Data Mining, KDD '16* (ACM, New York, NY, USA, 2016), pp. 785–794, 10.1145/2939672.2939785.
[31] See Supplemental Material at http://link.aps.org/supplemental/10.1103/v1q3-9dy8 for more details on the input variables and on the BDT architecture.
[32] L. Heinrich, M. Feickert, and G. Stark, PYHF: v0.7.6, 2024, https://doi.org/10.5281/zenodo.10470033.
[33] L. Heinrich, M. Feickert, G. Stark, and K. Cranmer, J. Open Source Software **6**, 2823 (2021).
[34] K. Cranmer and A. Held, EPJ Web Conf. **251**, 03067 (2021).
[35] A. L. Read, J. Phys. G **28**, 2693 (2002).
[36] G. Cowan, K. Cranmer, E. Gross, and O. Vitells, Eur. Phys. J. C **71**, 1554 (2011); **73**, 2501(E) (2013).
[37] Belle II Collaboration, HEPData record for this analysis, 10.17182/hepdata.159541 (2025).
[38] A. Pinto, Z. Wu, F. Balli, N. Berger, M. Boonekamp, E. Chapon, T. Kawamoto, and B. Malaescu, Eur. Phys. J. C **84**, 593 (2024).